Eur. Phys. J. B **44**, 423–430 (2005)
DOI: 10.1140/epjb/e2005-00141-4

THE EUROPEAN PHYSICAL JOURNAL B

Dynamic transition and hysteresis scaling in Heisenberg ferromagnet

Zhigao Huang[1,2,a], Fengming Zhang[2], Zhigao Chen[1,2], and Youwei Du[2]

[1] Department of Physics, Fujian Normal University, Fuzhou, 350007, China
[2] National Laboratory of Solid State Microstructures, Nanjing University, Nanjing 210093, China

Received 15 July 2004 / Received in final form 8 February 2005
Published online 30 May 2005 –

Abstract. Based on the mean-field treatment and Monte Carlo simulation, we studied the nature of the dynamic phase transition of two and three-dimensional magnetic films in Heisenberg model. The time averaged magnetization components (m_x, m_y, m_z),the average hysteresis-loop area components A for magnetic films with different thickness have been calculated. The dynamic transition phase diagrams from $Q = (1/\tau) \oint m(t)dt \neq 0$ to $Q = 0$ for the 2D and 3D cases have been obtained. The relaxation times for different values of magnetic field, temperature, thickness of the films and the orientation number of spin have been simulated. It is found that the loop area follows the scaling relation, $A - A_0 \propto H_0^{\alpha}\omega^{\beta}T^{-\gamma}$, and the exponents β and γ increase with increasing thickness, while the exponent α decreases with increasing thickness. It was observed that the phase boundary line shrinks inward in the H_0-T plane with decreasing value of the frequency of the magnetic field and thickness of multilayer film. The phase diagrams were explained by the competition between the relaxation time and the period of the external magnetic field. Moreover, it has been indicated that the dynamical behaviors for 2D and 3D cases derived by both mean-field method and Monte Carlo method in this work are consistent.

PACS. 75.60.Ej Magnetization curves, hysteresis, Barkhausen and related effects – 75.40.Mg Numerical simulation studies – 73.21.Ac Multilayers – 75.30.Kz Magnetic phase boundaries (including magnetic transitions, metamagnetism, etc.)

1 Introduction

Hysteresis is a characteristic of nonequilibrium phenomenon for metastable systems. If the applied magnetic field varies periodically in time, $H(t) = H_0 \sin \omega t$, the system is driven back and forth across a first-order phase transition at $H = 0$. As a result, $m(t)$ lags behind H(t), and the hysteretic effect takes place. The areas of the hysteresis loop, $A = \oint m(H)dH$, as functions of the amplitude H_0,frequency ω and temperature T have been studied in theory and experiment. Theoretical studies of hysteresis have been performed with several models [1–9], i.e. the mean-field treatments with Ising model [2–5], Monte Carlo simulations with Ising model [1,4–7], and O(N) type model [8,9]. The simulated average hysteresis-loop area showed a power scaling law, $(A - A_0) \propto H_0^{\alpha}\omega^{\beta}T^{-\gamma}$, where α, β and γ were the exponents depending on the dimensionality and symmetry of the system. However, different values of the exponents are predicted from various models. Recently, this scaling relation for the hysteresis loop area has been measured for several ultrathin and thin ferromagnetic film systems, such as, Fe/Au(001) [10], $Fe_{20}Ni_{80}$ [11], Co/Cu(001) [12,13], Fe/GaAs(001) [14] and Fe/W(110) [15] etc. The observed power scaling law in the experiments mentioned above was, in general, consistent with the simulated one [1–9]. However, there is much disagreement between theory and experiment for the values of the exponents α, β and γ. The disagreement may be attributed to the over-simplified treatment for the spins in Ising model. On the other hand, the dynamical behavior in Heisenberg model was simulated with Monte Carlo method [16,17]. Especially, Acharyya studied a off-axial dynamic symmetry breaking in uniaxially anisotropic Heisenberg ferromagnet and found that the transition temperature increases with the increase of the strength of anisotropy. However, no report appears in literature for the dynamical behavior from the mean-field treatment with Heisenberg model. So it is worth to investigate systematically the dynamical behaviors of the systems with Heisenberg model. In this paper, we focus on the nature of the dynamic phase transition of two and three-dimensional magnetic films with Heisenberg model using both the mean-field and Monte Carlo methods. The scaling exponents α, β and γ, and the dynamic phase diagrams for the magnetic films with different thickness,

[a] e-mail: zghuang@fjnu.edu.cn

frequency were investigated. The consistency of the results obtained from the mean-field method and Monte Carlo method is achieved, and the results agree generally with the reported experimental ones.

2 Model and simulation technique

By considering the classical Heisenberg exchange interactions between the spins in the $L \times L \times LN$ multilayer film in a magnetic field, the Hamiltonian of the system can be expressed as

$$H = -J \sum_{\langle ij \rangle} \overrightarrow{S}_i \cdot \overrightarrow{S_j} - K \sum_i (S_i^z)^2 - \overrightarrow{H}(t) \cdot \sum_i \overrightarrow{S}_i \quad (1)$$

where $\sum_{\langle ij \rangle}$ is performed over all the spin pairs at nearest-neighbor sites i and j with the exchange interaction J. K means the uniaxial anisotropy constant. $\overrightarrow{H}(t)$, aligning along the z axis, is the sinuous applied field, $\overrightarrow{H}(t) = \overrightarrow{H}'_0 \sin \omega t$. $\left|\overrightarrow{S}_i\right| = 1$ was set. J was taken as the unit of the temperature and energy, let $K = 1$. It was assumed that $L \times L \times LN$ multilayer films have the simple cubic lattices with $L = 20$ and LN , the number of the layers, variable. The periodic boundary conditions were applied in x and y axes. Meanwhile, the three-dimensional (3D) bulk was defined as a $L \times L \times L$ cube with $L = 20$ and the periodic boundary conditions in x, y and z axes were assumed.

Monte Carlo method with the metropolis algorithm for a classical Heisenberg system has been described in detail in [18–22]. In reference [22], different algorithms, such as the small trial step (STS), the uniform trial step (UTS), the reflection trial step (RTS) and the combined sampling were considered and it is found that the simulated results with UTS-algorithm are almost same as those with the combined sampling for the moderate value of anisotropy. In our simulation, UTS MC algorithm was used. One Monte Carlo step (MCS) is defined as a flip for every spin at the lattice sites, which is considered as the unit of the time in this simulation. For the numerical convenience, the magnetic field evolves periodically in a step-like sinuous fashion, which is similar to what described in [8]. It was defined that there are two time scales with unit in MCS for the sinuous magnetic field. One is N_m, the interval of time over which the field is a constant, another is $\tau = N_m \times N_l$ [17], the period of the magnetic field. Here, N_l means the number of intervals in a period of the magnetic field. In the simulation, let $N_l = 192$. We started from a random configuration in the high temperature region and had the system cooled quasicontinuously down to a measured temperature with zero magnetic field at a constant temperature step $T = -0.05\tilde{}-0.1$. 400 MCS were performed at each temperature. Then, the hysteresis loops were computed by starting from a demagnetized state at $H = 0$ and increasing quasicontinuously the magnetic field to H'_0, then decreasing to $-H'_0$. In order to get the stabilized states, the former 10 complete cycles of the oscillating field were discarded and the averages of various physical quantities were calculated from further 10 complete cycles.

The time averaged magnetization (over the complete cycle of the oscillating magnetic field), $Q = (1/\tau) \oint m(t) dt$, defines the dynamic order parameter [1,2,23], which was calculated for each period of the magnetic field. The magnetization $m(t)$ with a 200τ time series has been measured. For each temperature, the value of Q corresponding to each of the 200 cycles was calculated. Thus, based on those 200 different values of Q, the normalized statistics distribution $P(Q)$ with $\int P(Q) dQ = 1$ can be obtained. The fourth-order cumulation is defined as $U_L = 1.0 - \langle Q^4 \rangle / 3 \langle Q^2 \rangle^2$, where $\langle Q^n \rangle = \int Q^n P(Q) dQ$.

Next, we considered the mean-field treatment. The energy E_i at ith spin in the system with the classical Heisenberg model can be expressed as [24]

$$E_i = -\overrightarrow{S}_i \cdot \overrightarrow{H}_{eff} \quad (2)$$

where

$$\overrightarrow{H}_{eff} = J \sum_{j\{nn\}} \overrightarrow{S_j} + K \left(\overrightarrow{S}_i \cdot \overrightarrow{u}_i\right) \overrightarrow{u}_i + \overrightarrow{H}(t). \quad (3)$$

In the mean-field approximation, the first term in equation (3) can be approximately replaced by

$$J \sum_{j\{nn\}} \overrightarrow{S_j} = Za\overrightarrow{m} \quad (4)$$

where Z is the coordination number, a is a coefficient. $Z = 6$ and 4 correspond to three and two-dimensional (3D and 2D) cases for the simple cubic structure, respectively. According to the kinetic Bethe-Peierls approximation (KBPA) [4,25,26], the mean-field equation of motion of the average magnetization can be described by

$$\tau_t \frac{d\overrightarrow{m}}{dt} = \sum_i \overrightarrow{\Delta_i} \sum_{s_i \in \Delta} n\left(\overrightarrow{S}_i, \overrightarrow{m}\right) e^{-E_i(\overrightarrow{S}_i)/(k_B T')} \quad (5)$$

where τ_t is the microscopic (single spin-flip) relaxation time; $\overrightarrow{\Delta_i} = \overrightarrow{S}_i - \sum_i \overrightarrow{S}_i / N = \overrightarrow{S}_i - \overrightarrow{m}$, meaning the change in the state of the system associated with a spin flip event; $n(\overrightarrow{S}_i, \overrightarrow{m})$ is a combinatorial factor, which is the BPA to the number density of sites with local arrangements of spins $\overrightarrow{S}_i$ compatible with $\overrightarrow{\Delta}_i$ given as the system average magnetization is fixed at $\overrightarrow{m}$. It is reasoanable to assume that

$$n(\overrightarrow{S}_1, \overrightarrow{m}) = n(\overrightarrow{S}_2, \overrightarrow{m}) = \cdots = n(\overrightarrow{S}_N, \overrightarrow{m}) = \frac{1}{\sum_i e^{-E_i/(k_B T)}} \quad (6)$$

where $\overrightarrow{S}_1, \overrightarrow{S}_2, \cdots, \overrightarrow{S}_N$ are the orientations of the spin at every site, respectively. $\overrightarrow{S}_i$ was chosen according to

$$\overrightarrow{S}_i = \left(l_1 \overrightarrow{i} + l_2 \overrightarrow{j} + l_3 \overrightarrow{k}\right) / \left(l_1^2 + l_2^2 + l_3^2\right)^{0.5} \quad (7)$$

where $l_i(i=1,2,3) = -n, -(n-1), \cdots, (n-1), n$. Thus the number of orientations N for $\overrightarrow{S}_i$ is equal to $(2n+1)^3 - 1$. From equations (5) and (6), we can get

$$\tau_t \frac{d\overrightarrow{m}}{dt} = -\overrightarrow{m} + \frac{\sum_i \overrightarrow{S_i} e^{-E_i/(k_B T')}}{\sum_i e^{-E_i/(k_B T')}} \tag{8}$$

equation (8) can be rewritten as

$$\varpi \frac{d\overrightarrow{m}}{d\zeta} = -\overrightarrow{m} + \frac{\sum_i \overrightarrow{S_i} e^{-E_i/T}}{\sum_i e^{-E_i/T}} \tag{9}$$

where

$$E_i = -\overrightarrow{S}_i \cdot [Z(m_x \overrightarrow{i} + m_y \overrightarrow{j} + m_z \overrightarrow{k}) + k(\overrightarrow{S}_i \cdot \overrightarrow{u}_i)\overrightarrow{u}_i + \overrightarrow{H}_0 \sin(\zeta)] \tag{10}$$

where $k = K/a$, $\overrightarrow{H}_0 = \overrightarrow{H}'_0/a$, $T = k_B T'/a$, $\varpi = \omega\tau_t$ and $\zeta = \omega t$. It was assumed that a is used as unit of temperature and energy, and let $a = 1$. In the calculation, it was assumed that $\overrightarrow{u}_i$ and $\overrightarrow{H}_0$ are all along z axis, and let $k = 1.0$.

3 Simulated results and discussion

3.1 Monte Carlo simulation

In the simulation with Monte Carlo method, the hysteresis loops of multilayer films with $K = 1$, $LN = 1$, 3, 5, 7 and 3D bulk at different values of $N_m(\tau)$, H_0 and T were calculated. Figures 1a and b show the typical loops of multilayer films with $LN = 3$, $H_0 = 4.8$, $N_m = 2$, 50, 100, 300, 500, 1000, for $T = 0.1$, 0.5, respectively. As observed, at lower temperature ($T = 0.1$) an asymmetric loop ($Q > 0$) exists for $\tau = 384$ ($N_m = 2$); while for higher values of τ and higher temperature the symmetric loops are revealed. Moreover, it can be noted that the hysteresis loop areas increase with decreasing value of τ and temperature. Figure 2 shows the typical hysteresis loop areas as function of temperature with $LN = 3$, $\tau = 19\,200$, $H_0 = 0.6$, 1.2, 2.4, 4.8, 7.2, 9.6, 12.0 and 14.4, respectively. Obviously, for the low values of H_0 ($H_0 = 0.6$, 1.2 and 2.4) there is an abrupt change for the loop area, indicating a phase transition for Q from non-zero to zero. The areas of the hysteresis loops decrease with increasing temperature due to the decrease of the magnetization and coercivity as temperature is increased. Similarly, the relations between the hysteresis loop area and the frequency and amplitude of $H(t)$ for $LN = 3$ have also been calculated for different temperatures. Figure 3 shows the Ln-Ln plots of the areas to the field amplitude for $\tau = 19\,200$ and $T = 0.1$, 0.2, 0.3, 0.5, 0.7, 1.0, 1.5, respectively. It can be found that the value of Ln(A-A_0) increases linearly with increasing magnitude of Ln(H_0), which indicates an area scaling behavior (A-A_0) $\propto H_0^{\alpha}$. The slops of the straight lines yield the scaling exponent $\alpha = 0.38 \pm 0.02$, which

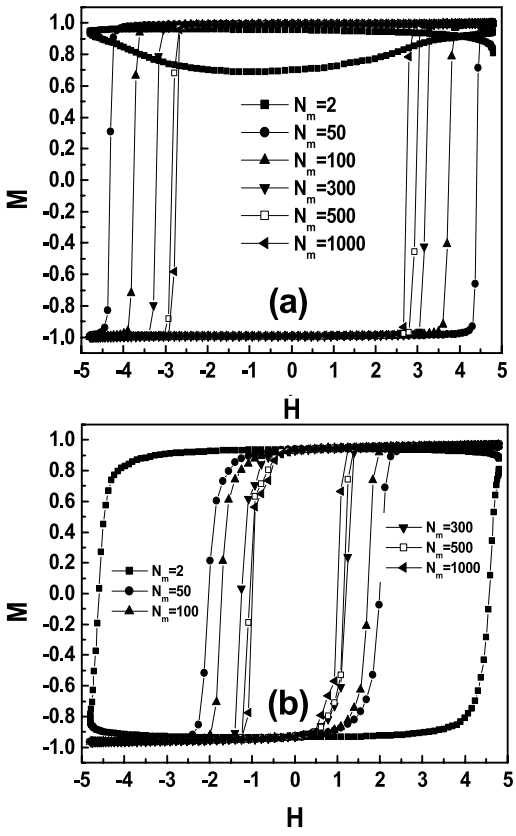

Fig. 1. The typical loops of multilayer film with $LN = 3$, $H_0 = 4.8$, $N_m = 2$, 50, 100, 300, 500, 1000, at (a) $T = 0.1$ and (b) $T = 0.5$, respectively.

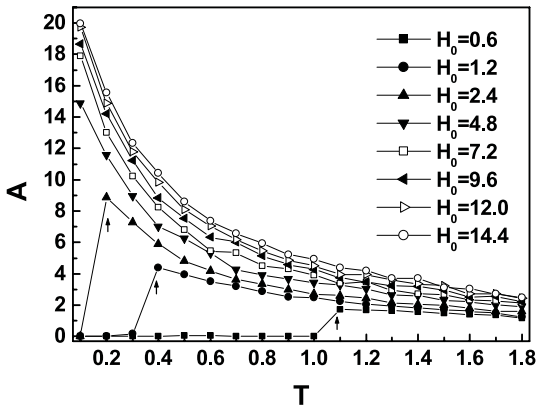

Fig. 2. The typical hysteresis loop areas as a function of temperature with $LN = 3$, $\tau = 19\,200$, $H_0 = 0.6$, 1.2, 2.4, 4.8, 7.2, 9.6, 12.0 and 14.4, respectively.

is, within error, independent of the temperature and frequency of the applied field. Shown in Figure 4 is the Ln-Ln plots of the loop area to the field frequency ($1/N_m$) for $H_0 = 4.8$, $T = 0.2$, 0.5, 1.0, 1.5, 1.8, respectively. Clearly, the value of Ln(A-A_0) increases linearly with increasing magnitude of Ln($1/N_{\rm m}$), which indicates a scaling behavior, (A-A_0) $\propto \omega^{\beta} = (1/(N \cdot N_{\rm m}))^{\beta}$, where $N = 192$. Similarly, the scaling exponent β was found as 0.41 ± 0.02. Figure 5 shows the Ln-Ln plots of the area to temperature

Table 1. The simulated exponents α, β and γ simulated by Monte Carlo (MC), Mean-field (MF), O(N), $(\Phi^2)^2$, and Landau-Ginzberg Hamiltonian methods, and the measured those from experiments.

Method	Thickness	α	β	γ	
MC Heisenberg	$LN = 1$(2D)	0.40 ± 0.02	0.38 ± 0.03	0.30 ± 0.02	This work
	$LN = 3$	0.38 ± 0.02	0.41 ± 0.02	0.60 ± 0.02	
	$LN = 5$	0.30 ± 0.02	0.45 ± 0.04	0.74 ± 0.02	
	$LN = 7$	0.30 ± 0.02	0.48 ± 0.04	0.77 ± 0.02	
	3D	0.30 ± 0.02	0.50 ± 0.03	0.80 ± 0.02	
MF Heisenberg ($\omega < \omega_{min}$)	2D	0.55 ± 0.04	0.40 ± 0.02	0.25 ± 0.02	This work
	3D	0.40 ± 0.04	0.60 ± 0.02	0.70 ± 0.02	
MF Heisenberg ($\omega = \omega_{min} \sim \omega_{max}$)	2D	1.35 ± 0.1	0.25 ± 0.03	0.25 ± 0.02	
	3D	0.95 ± 0.05	0.25 ± 0.03	0.70 ± 0.02	
MC Ising	2D	0.70	0.36	1.18	[6]
	3D	0.67	0.46	1.98	
	$4D$	0.32	0.52		
L-G Hamiltonian Ising	2D		0.41 ± 0.01		[25]
	3D		0.50 ± 0.01		
3D O(N)		0.50	0.50		[26]
3D$(\Phi^2)^2$		0.66 ± 0.05	0.33 ± 0.03	0.7	[3,8,9]
Ni-Fe (Exp.)	Thickness = 200 Å	0.900 ± 0.002	0.800 ± 0.002	0.38 ± 0.01	[11]
Fe-Au (Exp.)	$1.5 \sim 3.3$ ML	0.59 ± 0.07	0.31×0.05		[10]
Co-Cu (Exp.)	3.0 ML	0.67 ± 0.01	0.67 ± 0.03		[12]

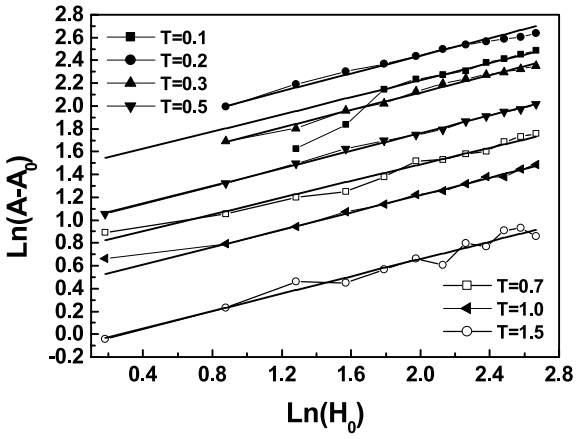

Fig. 3. The Ln-Ln plots of the hysteresis loop areas to the field amplitude for $\tau = 19\,200$, $T = 0.1$, 0.2, 0.3, 0.5, 0.7, 1.0, 1.5, respectively.

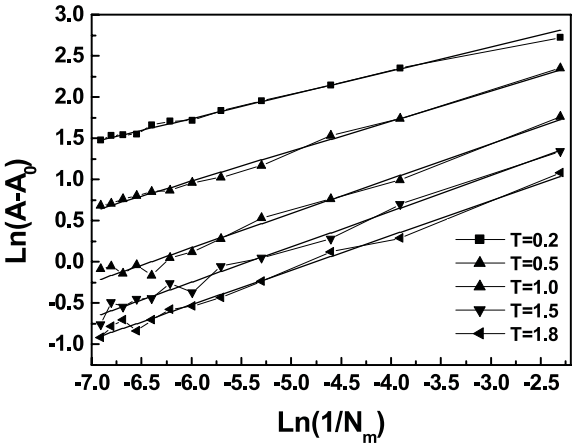

Fig. 4. The Ln-Ln plots of the hysteresis loop areas to the field frequency $(1/N_m)$ for $H_0 = 4.8$, $T = 0.2$, 0.5, 1.0, 1.5, 1.8, respectively.

for $H_0 = 4.8$, $N_{\rm m} = 4$, 10, 50, 100, 500, 1000, respectively. The linear variation of Ln(A-A_0) versus Ln(T) yields the scaling exponent $\gamma = 0.60 \pm 0.02$. In low frequency and low temperature regions, especially for $N_m = 4$, 10, the deviation from the linearity is attributed to the appearance of the phase with $Q \neq 0$, as seen in Figure 5. Furthermore, the hysteresis loops and their areas of multilayer films for $LN = 1$, 5, 7 and 3D have also been calculated and the scaling relations, $(A\text{-}A_0) \propto H_0^{\alpha} \omega^{\beta} T^{-\gamma}$, were obtained. For summary, the simulated exponents α, β and γ to system with different thickness are listed in Table 1.

3.2 Calculation on mean-field equation of motion

In solving equation (9) by the fourth–order Runge-Kutta method, 11 periods were considered. Discarding the first 5 periods, the stationary solutions, the instantaneous values of the magnetization components $M_x(\zeta)$, $M_y(\zeta)$ and $M_z(\zeta)$, were calculated as the parameters T, H_0 and ϖ were taken at the fixed values. It was observed that the magnitude of n influences evidently the solutions of equation (9), $M_x(\zeta)$, $M_y(\zeta)$ and $M_z(\zeta)$. However, it has been found that, when $n \geq 8$, the solutions $M_x(\zeta)$, $M_y(\zeta)$ and $M_z(\zeta)$ hardly depend on the value of n and arrive at

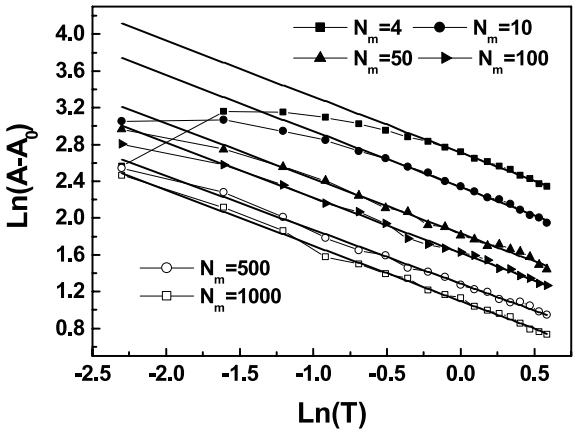

Fig. 5. The Ln-Ln plots of the hysteresis loop areas to the temperature for $H_0 = 4.8$, $N_{\rm m} = 4$, 10, 50, 100, 500, 1000, respectively.

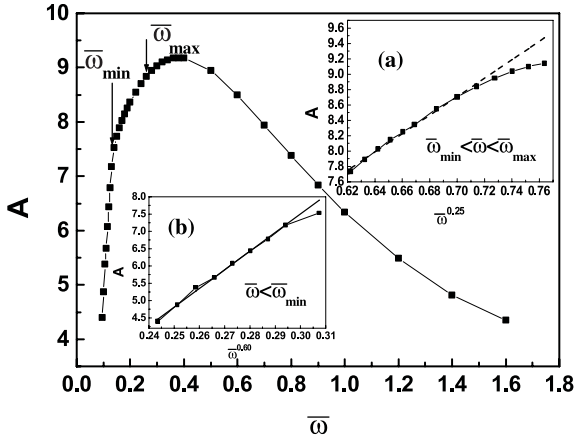

Fig. 6. The typical value of A as a function of ϖ for $z = 6$, $k = 1$, H_0=4.0.

the stationary values. In the calculation, only the case for $n = 10$ was studied typically. Figure 6 shows the typical value of A as a function of ϖ for $z = 6$, $k = 1$, $H_0 = 4.0$. From the figure, it is found that there exists a complicated relation between A and ϖ. Here, we focused on the low frequency region. The $A \sim \varpi$ curve corresponds to different scaling relations in different frequency regions. As shown in insets (a) and (b) of the figure, as ϖ is between $\varpi_{\rm min} \sim \varpi_{\rm max}$, the scaling relation, $(A\text{-}A_0) \propto \varpi^{\beta}$, with $\beta = 0.25 \pm 0.02$ is obtained; while as $\varpi < \varpi_{\rm min}$, the scaling relation with $\beta = 0.60 \pm 0.06$ is observed. Here $\varpi_{\rm max}$, $\varpi_{\rm min}$ are the high and low limits of the frequency for β being kept as a constant within error, respectively. Figure 7 shows the typical hysteresis loop area A as function of $T^{-\gamma}$ for $z = 6$, $H_0 = 1.0$ and 2.0, $\varpi = 0.1$ and 0.2, respectively. The linear variation of $(A\text{-}A_0)$ versus $T^{-\gamma}$ yields the scaling exponent $\gamma = 0.70 \pm 0.05$ for low frequency region, which is independent of the values of ϖ and H_0 within error. Shown in Figures 8a and b, are the typical hysteresis loop area A as a function of H_0^{α} for $z = 6$, $T = 2.0$, 2.2 and 2.4, $\varpi = 0.1$, 0.12 ($\varpi < \varpi_{\rm min}$), and $\varpi = 0.14$, 0.16, 0.20 and 0.24 ($\varpi = \varpi_{\rm min} \sim \varpi_{\rm max}$), re-

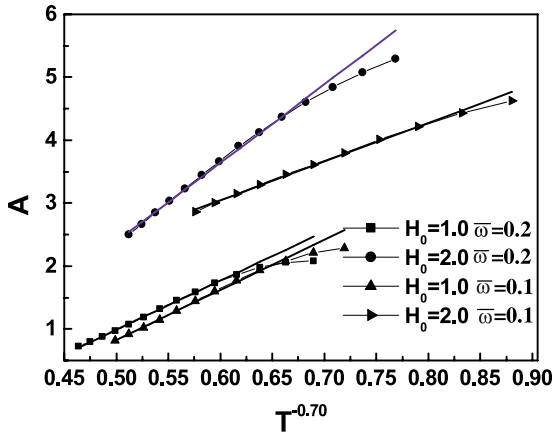

Fig. 7. The typical hysteresis loop area A as a function of $T^{-\gamma}$ for $z = 6$, $H_0 = 1.0$ and 2.0, $\varpi = 0.1$ and 0.2, respectively.

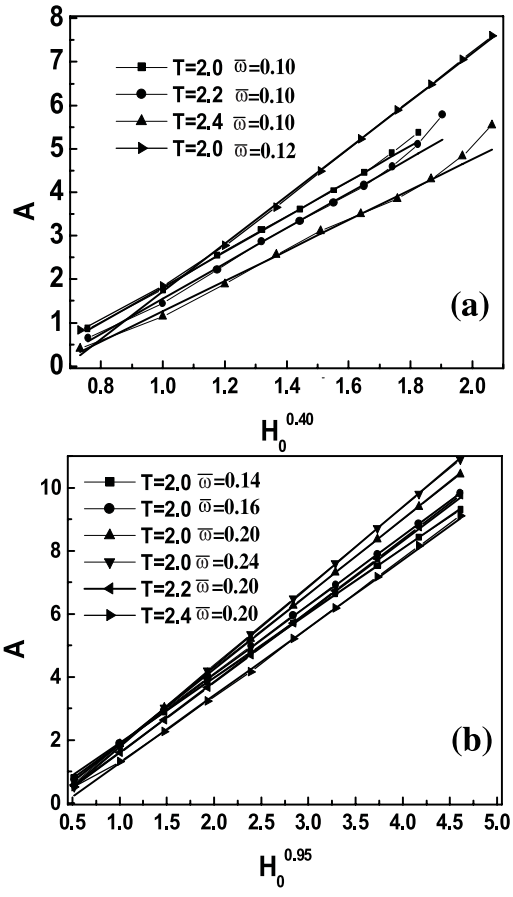

Fig. 8. The typical hysteresis loop area A as a function of H_0^{α}. (a) for $z = 6$, T=2.0, 2.2 and 2.4, $\varpi = 0.1$, 0.12 ($\varpi < \varpi_{\rm min}$); (b) for z=6, T=2.0, 2.2 and 2.4, and $\varpi = 0.14$, 0.16, 0.20 and 0.24 ($\varpi = \varpi_{\rm min} \sim \varpi_{\rm max}$), respectively.

spectively. The linear variations of $(A\text{-}A_0)$ versus H_0^{α} yield the scaling exponents $\alpha = 0.40 \pm 0.04$ for $\varpi < \varpi_{\rm min}$ and $\alpha = 0.95 \pm 0.05$ for $\varpi = \varpi_{\rm min} \sim \varpi_{\rm max}$, which is independent of the values of ϖ and T within error. Similar scaling behavior for $z = 4$ has also been observed and the scaling exponents α, β and γ are listed in Table 1.

From Table 1, it is found that exponents β and γ increase with increasing thickness. In contrast, exponent α

decreases with increasing thickness. Moreover, it can be found that with mean-field method and Monte Carlo method the values of β and γ for 2D and 3D cases are in agreement. For lower frequency ($\varpi < \varpi_{\min}$), the values of α for 2D and 3D cases from mean-field method are near to those from Monte Carlo. However, for $\varpi = \varpi_{\min} \sim \varpi_{\max}$, the values of α from the mean-field method are much larger than those from Monte Carlo method, which will be studied further. The above scaling behaviors are similar to those for Ising model and experimental results [1–15,17,27]. The trend of changes of α, β and γ with the dimension number in Heisenberg model is similar to that in other models [3,6,28–30]. As the dimension is changed from 2D to 3D, the value of α is decreased from 0.40 to 0.30 (MC) or 0.55 to 0.40 (MF) in Heisenberg model, which is similar to that it is reduced from 0.70 to 0.67 in Ising model. Similarly, the value of β increases from 0.38 to 0.50 (MC) or 0.40 to 0.60 (MF) in Heisenberg model, which is similar to that it does from 0.36 to 0.45 in Ising model too. The magnitude of γ increases from 0.30 to 0.80 (MC) or 0.25 to 0.70 (MF) in Heisenberg model, further consistent with the change trend from 1.18 to 1.98 for Ising model [6]. However, the values of γ from Ising model are much larger than those from Heisenberg model. Although the magnitudes of the scaling exponents α, β and γ obtained from different models and experiments are quite different, the obtained results in this work are self-consistent. The values of β ($\beta = 0.25 \sim 0.60$) are consistent with the experiment scaling exponents, $\beta = 0.31$ in an Fe/Au(001) [10], $\beta = 0.325 \sim 0.399$ at high sweep rates in expitaxial Fe/GaAs(001) [14], and the theoretical predictions for a continuous spin system, such as $\beta = 0.5$ in [28–30] and $\beta = 0.33$ [3]. Similarly, the values of α ($\alpha = 0.30 \sim 0.55$) for low frequency region are consistent with the experiment scaling exponents, $\alpha = 0.59$ in an Fe/Au(001) film [10], $\alpha = 0.67$ in Co/Cu(001) thin films [12], $\alpha = 0.25$ in Fe/W(001) thin films [13] and the theoretical predictions for a continuous spin system,such as $\alpha = 0.5$ in [28–30] and $\alpha = 0.67$ [3]. Also, the values of γ ($\gamma = 0.30 \sim 0.80$) are consistent with the experiment scaling exponents, $\gamma = 0.38$ in an $Cu/Ni_{80}Fe_{20}/Si(001)$ film [11], and the theoretical predictions $\gamma = 0.7$ for a continuous spin system [3,8,9].

3.3 Phase diagram and relaxation time

In Monte Carlo simulation, a minimum in $U_L \sim T$ curve is used as a criterion of the transition between $Q \neq 0$ and $Q = 0$. The simulated deep minima in $U_L \sim T$ curves for various τ, H_0 and LN have been obtained, indicating a transition of first-order with the transition point from $Q \neq 0$ to $Q = 0$ at minimum. Figure 9 shows the dynamic phase transition diagrams for the multilayer films with $LN = 1$, 3, 5 and 3D, $\tau = 100, 1000$ and 19 200, respectively. In mean-field calculation, $M_z(\zeta)$-H loop is asymmetric at low temperature and correspondent $Q \neq 0$, while at higher temperature $M_z(\zeta)$-H loop is symmetric and $Q = 0$. A dynamic transition temperature T_C is defined by the position of peak in the $dQ/dT - T$ curve.

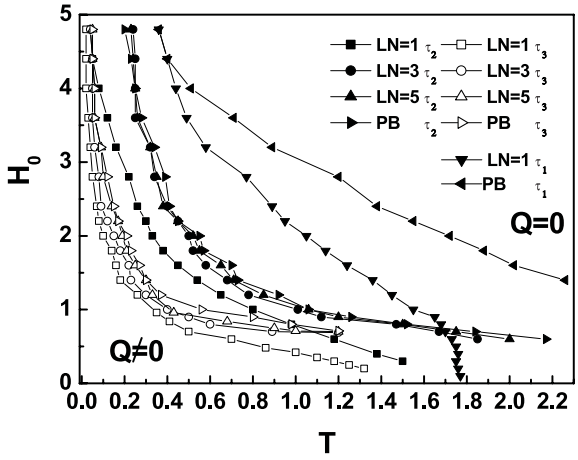

Fig. 9. The dynamic phase diagrams obtained with MC simulation for the multilayer films with LN=1, 3, 5 and 3D, $\tau_1 = 100$, $\tau_2 = 1000$ and $\tau_3 = 19\,200$, respectively.

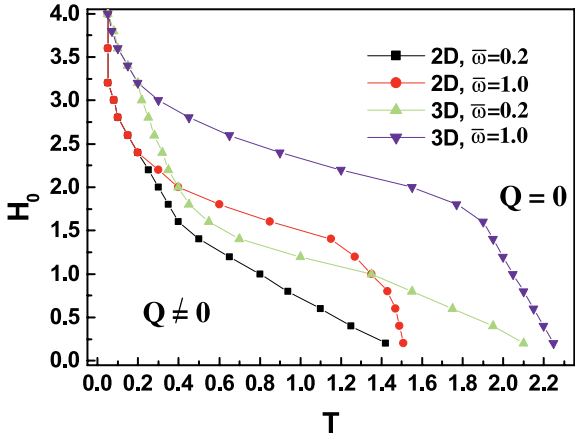

Fig. 10. The phase transition diagrams obtained with MF calculation with $\varpi = 0.2$ and 1.0 for the 2D and 3D cases, respectively.

According to the value of T_c, the phase transition diagrams, indicating the regions of $Q \neq 0$ and $Q = 0$, for H_0-T with $\varpi = 0.2$ and 1.0 for the 2D and 3D cases are shown in Figure 10, respectively. From Figures 9 and 10, it is found that the phase diagram derived by mean-field method is consistent with that by Monte Carlo method, and in the H_0-T plane the phase boundary line shrinks inward with decreasing value of ω ($=1/\tau$) and ϖ, which is similar to those in Ising model [6]. Also, it is observed that the phase transition curves shift to the right as the multilayer number LN increases or the dimensionality changes from two to three.

Now we explain the phase diagrams based on the competition between the intrinsic relaxation lifetime (or effective time lag) τ_r [6] and the period of the external magnetic field $\tau(\sim 2\pi/\omega)$. The relaxation time is described by the expression $\tau_r = \tau_{r0} \exp(\Delta U/k_B T)$ with $\Delta U = KV[1-(H + H_{int} + \lambda M)/H_c]^2$ [31–33]. Here, H, H_{int} and λM are the applied magnetic field, the local interaction field and the mean field, respectively. So the relaxation time τ_r is associated with the magnetic interaction, the applied

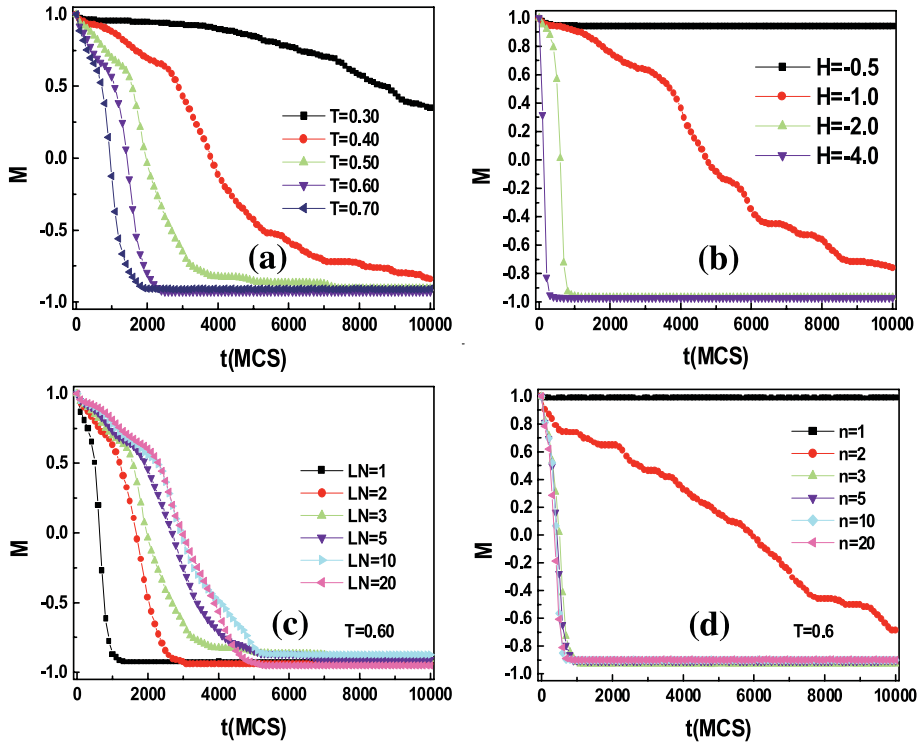

Fig. 11. The magnetization as a function of time for the films, (a) for $LN = 3$, $n = 10$, $H = -1.0$, $T = 0.30$–0.70; (6) for $LN = 5$, $n = 10$, $T = -0.6$, $H = -0.5$, –1.0, –2.0, –4.0; (c) for $T = 0.60$, $n = 10$, $H = -1.0$, $LN = 1$, 2, 3, 5, 10, 20; (d) for $LN = 1$, $T = 10$, $H = -1.0$, $n = 1$, 2, 3, 5, 10, 20, respectively.

field, the temperature and the anisotropy in the films. It was assumed that the initial state of spin at every site for the films is $S_z = 1$. When a magnetic field H along $-z$ axis is applied, the magnetization of the film will gradually orientate along $-z$ axis with increasing time (unit in MCS). The relaxation time was taken as time in which the magnetization is changed from $+1$ to $+\exp(-1)$. In order to study the influence of the orientation number n on the relaxation time, the orientations of the spin determined by equation (7) were used in updating the spin configuration.

Figure 11a–d show the magnetization as a function of time (unit with MCS in MC simulation) for the films with different temperature T, magnetic field H, thickness LN and orientation number of spin n, respectively. From the figure, it can be found easily that the relaxation time decreases with increasing values of T, H, n and with decreasing coordinate number (or LN), which is similar to those in Ising model [34–36]. The phase boundary line can be considered as a result of the competition between the relaxation time τ_r and the period of the external magnetic field τ. When τ_r is less than τ, there is enough time for the magnetization to change its sign, and consequently the symmetrical hysteresis loop can appear and $Q = 0$. In contrast, the magnetization can not fully change its sign due to with no enough time when τ_r is larger than τ, consequently the asymmetrical hysteresis loop can be found and $Q \neq 0$. For the same $\omega(\varpi)$, n and z, it is assumed that the value of τ_r is always equal to the fixed value of τ at the same boundary line. Thus, when the temperature decreases, the value of H_0 has to increase in order to remain the value of τ_r to be unchanged. Therefore, the value of τ increases sharply with decreasing temperature in the low temperature region and consequently the value of H_0 has to rise rapidly. The large slope of the boundary curves at low temperature, as seen in Figures 9 and 10, can be explained satisfactorily. For the same H_0, n and z, the larger the value of ϖ, the less the magnitude of τ_r is. So the phase boundary line with the larger value of ϖ need to shift to higher temperature region for the less relaxation time. In order to keep the value of τ_r to be unchanged, the increase of τ_r resulted from higher z has to be compensated by the increasing temperature. Therefore, for the same H_0, n and ϖ, the phase boundary line with the large value of z should shift to the higher temperature region.

4 Conclusion

In conclusion, the mean-field equations of motion of the magnetization with Heisenberg model were established. The dynamic scaling behavior and phase transition of the two and three-dimensional Heisenberg magnetic films were studied by the mean-field treatment and Monte Carlo simulation. The dynamic transition phase diagrams H_0-T from $Q = 0$ to $Q \neq 0$ for the 2D and 3D cases were obtained. The scaling exponents α, β and γ for the magnetic films with different thickness were obtained. It is found that the exponents β and γ increase with increasing thickness. In contrast, the exponent α decreases with increasing

thickness. Moreover, the values of β, γ and α (in lower frequency) for 2D and 3D cases obtained by the mean-field method are consistent with those by Monte Carlo method. The scaling behaviors are similar to those for other models reported, and give consistent results. It is found that the phase boundary line in the H_0-T plane shrinks inward with decreasing value of ω $(=1/\tau)$, ϖ and thickness of multilayer film. MC simulated results indicated that the relaxation time decreases with increasing values of T, H, n and with decreasing coordinate number (or LN). The phase diagrams have been explained satisfactorily from the competition between the relaxation time τ_r and the period of the external magnetic field τ.

This work was supported by Grants No.G1999064508 for National Key Project for Basic Research of China, and Foundation for University Key Teacher by the Ministry of Education, and NSF of Fujian Province (E0320002), and NSF of China by Grant No.10474037.

References

1. B.K. Chakrabarti, M. Acharyya, Rev. Mod. Phys. **71**, 847 (1998)
2. T. Tome, M.J. de Oliveira, Phys. Rev. A **41**, 4251 (1990)
3. M. Rao, H.R. Krishnamurthy, R. Pandit, Phys. Rev. B **42**, 856 (1990)
4. C.N. Luse, A. Zangwill, Phys. Rev. E **50**, 224 (1994)
5. M. Acharyya, Phys. Rev. E **58**, 179 (1998)
6. M. Acharyya, B.K. Chakrabarti, Phys. Rev. B **52**, 6550 (1995)
7. W.S. Lo, R.A. Pelcovits, Phys. Rev. A **42**, 7471 (1990)
8. M. Rao, H.R. Krishnamurthy, R. Pandit, J. Phys: Condens. Matter **1**, 9061 (1989)
9. M. Rao, R. Pandit, Phys. Rev. B **43**, 3373 (1991)
10. Y.L. He, G.C. Wang, Phys. Rev. Lett. **70**, 2336 (1993)
11. B.C. Choi, W.Y. Lee, A. Samad, J.A.C. Bland, Phys. Rev. B **60**, 11906 (1999)
12. Q. Jiang, H.N. Yang, G.C. Wang, Phys. Rev. B **52**, 14911 (1995)
13. Jih-Shin Suen, M.H. Lee, G. Teeter, J.L. Erskine, Phys. Rev. B **59**, 4249 (1999)
14. W.Y. Lee, B.Ch. Choi, Y.B. Xu, J.A.C. Bland, Phys. Rev. B **60**, 10216 (1999)
15. Jih-Shin Suen, J.L. Erskine, Phys. Rev. Lett. **78**, 3567 (1997)
16. M. Acharyya, Int. J. Mod. Phys. C **12**, 709 (2001)
17. H. Jang, M.J. Grimson, Phys. Rev. E **63**, 066119 (2001)
18. K. Binder, D.W. Heermann, *Monte Carlo Simulation in Statistical Physics* (Springer, Berlin, 1992)
19. Zhigao Huang, Zhigao Chen, Fengming Zhang, Youwei Du, Eur. Phys. J. B **37**, 177 (2004)
20. Zhigao Huang, Youwei Du, Phys. Lett. A **300**, 641 (2002)
21. Zhigao Huang, Zhigao Chen, Kun Peng, Dunhui Wang, Fengming Zhang, Weiyi Zhang, Youwei Du, Phys. Rev. B **69**, 094420 (2004)
22. D. Hinzke, U. Nowak, Comp. Phys. Commun. **121-122**, 334 (1999)
23. M. Acharyya, Phys. Rev. E **59**, 218 (1999)
24. R.H. Kodaman, A.E. Berkowitz, Phys. Rev. B **59**, 6321 (1999)
25. C.N. Luse, A. Zangwill, J. Appl. Phys. **79**, 4942 (1996)
26. Y. Saito, R. Kubo, J. Status Phys. **15**, 233 (1976)
27. G.P. Zheng, J.X. Zhang, Phys. Rev. E **58**, R1187 (1998)
28. D. Dhar, P.B. Thomas, J. Phys. A **25**, 4967 (1992); 26, 3973 (1993)
29. F. Zhong, J.X. Zhang, Phys. Rev. Lett. **75**, 2027 (1995)
30. A.M. Somoza, A.C. Desai, Phys. Rev. Lett. **70**, 3279 (1993)
31. A.F. Khapikov, S. Wang, B. Xu, J.W. Harrell, Phys. Rev. B **63**, 020401(R) (2000)
32. P. Zhang, F. Zuo, F.K. Urban III, A. Khabari, P. Griffiths, A. Hosseini-Tehrani, J. Magn. Magn. Mater. **225**, 337 (2001)
33. B. Raquet, M.D. Ortega, M. Goiran, A.R. Fert, J.P. Redoules, R. Mamy, J.C. Ousset, A. Sdaq, A. Khmou, J. Magn. Magn. Mater. **150**, L5 (1995)
34. P.A. Rikvold, H. Tomita, S. Miyashita, S.W. Sides, Phys. Rev. E **49**, 5080 (1994)
35. G. Korniss, C.J. White, P.A. Rikvold, M.A. Novotny, Phys. Rev. E **63**, 016120-1 (2000)
36. K. Brendel, G.T. Barkema, H. Beijeren, Phys. Rev. E **67**, 026119 (2003)